The solution structure of the viral binding domain of Tva, the cellular receptor for subgroup A avian leukosis and sarcoma virus[1]

Marco Tonelli[c], Reuben J. Peters[b,2], Thomas L. James[c], David A. Agard[a,b,c,*]

[a] *The Howard Hughes Medical Institute, University of California, San Francisco, CA 94143, USA*
[b] *Department of Biochemistry and Biophysics, University of California, San Francisco, CA 94143, USA*
[c] *Department of Pharmaceutical Chemistry, University of California, San Francisco, CA 94143, USA*

Received 24 September 2001; revised 22 October 2001; accepted 23 October 2001

First published online 19 November 2001

Edited by Gunnar von Heijne

Abstract The cellular receptor for subgroup A avian leukosis and sarcoma virus (ALSV-A) is Tva, which contains a motif related to repeats in the low density lipoprotein receptor (LDLR) ligand binding repeat (LBr) and which is necessary for viral entry. As observed with LBr repeats of LDLR, the 47 residue LBr domain of Tva (sTva47) requires calcium during oxidative folding to form the correct disulfide bonds, and calcium enhances the structure of correctly oxidized sTva47, as well as its ability to bind the viral envelope protein (Env). However, solution nuclear magnetic resonance studies indicate that, even in the presence of excess calcium, sTva47 exists in an ensemble of conformations. Nonetheless, as reported here, the structure of the predominant sTva47 solution conformer closely resembles that of other LBr repeats, with identical S–S binding topology and octahedral calcium coordination. The location of W48 and other critical residues on the surface suggests a region of the molecule necessary for Env binding and to mediate post-binding events important for ALSV-A cell entry.

Key words: Viral receptor; Viral cell entry; Low density lipoprotein receptor; Nuclear magnetic resonance structure; Conformational heterogeneity

1. Introduction

Enveloped viruses must fuse their viral membrane with the membrane of the host cell to initiate a productive infection. In retroviruses this membrane fusion is carried out by the viral envelope fusion glycoprotein (Env), which is composed of surface (SU) and transmembrane (TM) subunits that form a trimer of SU/TM heterodimers. Env binds to cellular receptors through the SU subunit, mediating viral attachment, and generally defining target specificity. In many cases, following the initial interaction between Env and a cellular receptor, internalization from the cell surface is triggered by interaction with another cellular receptor (e.g. the human immunodeficiency virus) or through endosomal internalization. A two-step conformational change mechanism is generally involved in converting Env to the fusogenic state. Initially, the surface subunits are partially disassembled (either by receptor binding or reduction in pH in an endosomal compartment), which act to prime Env to undergo further conformational change. Final conversion to the fusogenic state is mediated by interaction with an additional receptor or a (further) drop in pH [1].

By contrast with the influenza A virus, which, upon endosomal internalization, uses the decrease in pH to trigger viral entry [2,3], most retroviruses are believed to use a pH-independent mechanism where receptor binding directly triggers viral entry. Because of its apparent simplicity (i.e. utilization of a single receptor), the avian leukosis sarcoma virus (ALSV) has become a model system to study pH-independent viral cell entry. Surprisingly, recent data suggest that, for ALSV cell entry, receptor binding must be followed by a decrease in pH [4]. In any case, for ALSV, receptor binding serves to drive conformational changes necessary for viral cell entry.

The ALSV family is comprised of five major subgroups (A–E), that differ in host range, receptor binding, and interference patterns [5]. The receptor for subgroup A ALSV (Tva) has been cloned from both quail [6] and chicken [7] and shown to be necessary for ALSV-A cell entry [7]. Tva encodes a small (83 amino acids (aa)) ectodomain that contains a single copy of a cysteine-rich motif first identified as seven repeats in the ligand binding domain of the low density lipoprotein receptor (LDLR) [6]. This ~40 aa LDLR ligand binding repeat (LBr) is sufficient to reconstitute ALSV-A cell entry [8]. Mutational analysis of the cysteines in the Tva LDLR LBr suggested a first–third, second–fifth, and fourth–sixth disulfide bonding pattern [9], which matches that later determined for the LBr of LDLR [10–12]. Intriguingly, further mutational analysis has suggested that tryptophan 48 (W48) serves a critical role in post-binding events required for the viral fusion protein to assume a liposome binding conformation [13] and for viral cell entry [14].

*Corresponding author. Fax: (1)-415-476 1902.
E-mail address: agard@msg.ucsf.edu (D.A. Agard).

[1] Numbering is based on the full length Tva receptor.
[2] Present address: Institute of Biological Chemistry, Washington State University, Pullman, WA 99164-6340, USA.

Abbreviations: ALSV-A, subgroup A avian leukosis and sarcoma virus; Tva, receptor for ALSV-A; aa, amino acid; sTva, soluble Tva ectodomain; sTva47, 47 aa soluble Tva LBr; Env, viral envelope fusion glycoprotein; SU, surface subunits of Env; TM, transmembrane subunits of Env; SU(A)-rIgG (SU(A)-immunoadhesin), soluble fusion of ALSV-A Env SU to constant region of immunoglobulin G; LDLR, low density lipoprotein receptor; LBr, ligand binding repeat of LDLR; MBP, maltose binding protein; MBP–sTva47, fusion of sTva47 to MBP; HBS, HEPES-buffered saline; EDTA, ethylenediaminetetraacetate; NMR, nuclear magnetic resonance; 2D, two-dimensional; 3D, three-dimensional; HSQC, heteronuclear single quantum coherence spectra; NOE, nuclear Overhauser enhancement; NOESY, NOE spectroscopy; rmsd, root mean square deviation

0014-5793/01/$20.00
PII: S0014-5793(01)03086-1

The binding of low density lipoprotein to the LDLR is dependent on the presence of calcium [15]. Further, the LBr of LDLR receptor family requires calcium during oxidative folding to selectively form the correct disulfide bonds [11,16–18] and calcium stabilizes their structures [19–22]. We have shown a similar requirement for calcium in the bacterially expressed soluble Tva LBr (sTva47) from the quail sequence. Calcium was necessary for the selective formation of the correct disulfide bonds during oxidative folding and enhanced its structural stability, as also observed by Wang et al. [23]. We have also measured the binding of sTva47 to an ALSV-A SU-immunoadhesin to be enhanced ~30-fold by the presence of calcium.

In this communication we present the three-dimensional (3D) structure of the major solution conformation assumed by sTva47 with excess calcium, solved using heteronuclear nuclear magnetic resonance (NMR) techniques. Not surprisingly, we found that it closely resembles that of LDLR LBr domains, especially in the C-terminal half that shows the most sequence similarity and contains a calcium binding site. In fact, although calcium was not explicitly included during structural refinement, the four conserved acidic side chains and two backbone carbonyl oxygen atoms were restricted by the NMR restraints to a correct position for octahedral coordination. The structure reveals that residues known to be important for binding comprise and cluster around a hydrophobic patch on the receptor surface.

2. Materials and methods

2.1. Construction of sTva expression vectors

The quail Tva LDLR LBr (Tva residues 11–51, Fig. 1) was subcloned into pBluescript (Stratagene) using PCR to introduce an in-frame 5′ *Bam*HI and 3′ stop codon and *Eco*RI site. These restriction sites were further used to subclone into pET12a (Stratagene) or maltose binding protein (MBP)-fusion pMAL (New England Biolabs) vectors. All constructs were verified by sequencing.

2.2. Expression and purification of MBP–sTva47

The cytoplasmic MBP–sTva47 fusion yielded the best expression (~40% of total soluble protein) and was subsequently utilized, although the subcloning protocol leaves six residues (ISEFGS) on the N-terminus of the 41 aa Tva LBr after factor Xa release from MBP. Expression and purification were performed essentially following the recommended protocol. However, it was necessary to incorporate an anion exchange step prior to affinity purification. Clarified extract was loaded onto a HiTrap Q column (Pharmacia), washed and eluted with a 0–1 M NaCl gradient (MBP–sTva47 elutes in a broad peak from 150 to 450 mM). Because approximately half of the total expressed MBP–sTva47 is found in the flow through and wash from the amylose (affinity) column, these were combined, diluted 1:1 with buffer, and rerun over the HiTrap Q and amylose columns, as above.

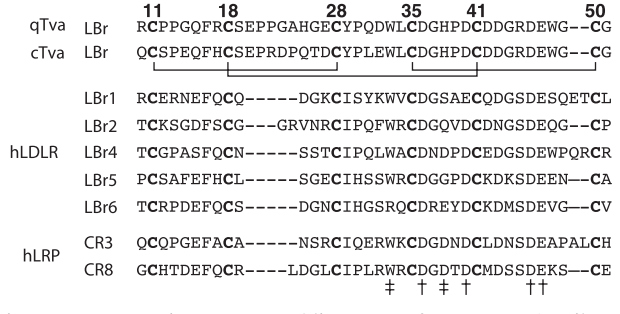

Fig. 1. Tva contains an LBr. Alignment of Tva LBr (quail and chicken, qTva and cTva, respectively) with previously characterized LBr from human LDLR (hLDLR) and human LDLR-related protein (hLRP). Conserved cysteines characteristic of LBr are in bold with the disulfide bond pairings connected above the alignment. The daggers below the alignment indicate the residues involved in calcium chelation (‡, coordination by backbone carbonyl; †, coordination by side chain carboxyl) as suggested by the crystal structure of hLDLR LBr5 [21].

2.3. Oxidation and proteolytic release of sTva47

Oxidation of sTva47 was routinely performed in the context of the fusion protein. Purified MBP–sTva47 was diluted to $A_{280} = 0.5$ with buffer and oxidized by the addition of 3 mM reduced glutathione, 0.3 mM oxidized glutathione, and 5 mM $CaCl_2$, followed by incubation at 4°C for at least 12 h [10–12]. Oxidized sTva47 could be released from MBP with factor Xa (New England Biolabs) cleavage and separated by ultrafiltration through a 10 kDa molecular weight cutoff membrane (Amicon). The released sTva47 in the filtrate was then polished on a preparative scale C18 reversed phase column (Vydac) using a Pharmacia AKTA HPLC. Fractions containing sTva47 (>99% purity as judged by electrospray mass spectrometry) were pooled and lyophilized. This lyophilized protein was brought up into the appropriate buffers and concentrations determined using the calculated extinction coefficient, $\varepsilon = 12\,900\ M^{-1}\ cm^{-1}$.

2.4. Surface plasmon resonance binding studies

Binding studies were carried out using a BIAcore (BIAcore AB) with the MBP–sTva47 fusion immobilized (the relatively much larger MBP provided a means to leave sTva47 largely free of potentially interfering surface effects). Oxidized MBP–sTva47 was immobilized following the recommended protocol (Pharmacia BioSensor). All binding experiments were performed using degassed and 0.2 μ filtered HEPES-buffered saline (HBS; 10 mM HEPES, 150 mM NaCl) and either 2.5 mM EDTA (ethylenediaminetetraacetate) or 5 mM $CaCl_2$, with freshly added 0.0005% P20 surfactant, as the running buffer. ALSV-A SU-immunoadhesin (SU(A)-rIgG) fusion protein was dialyzed into HBS+2.5 mM EDTA and diluted five-fold into either the same or HBS+5 mM $CaCl_2$ and the concentration determined by A_{280} using the calculated extinction coefficient, $\varepsilon = 99\,920\ M^{-1}\ cm^{-1}$ (P20 surfactant was added to 0.0005% prior to use). Injections of 10 mM HCl were used to regenerate the binding surfaces before and between injections of SU(A)-rIgG.

2.5. NMR structural determination of sTva47

Labeled sTva47 was obtained from expression in appropriately labeled minimal media (M9) culture. Expression, purification, and oxidation were carried out as described above. An NMR sample was then prepared with ~2 mM ^{15}N,^{13}C-labeled sTva47 in 50 mM d_3-Na-acetate, 5 mM $CaCl_2$ and 10% D_2O at pH 5.5. Preliminary NMR experiments were carried out a Bruker DMX 600 MHz spectrometer, while standard two-dimensional (2D) and 3D heteronuclear experiments for structure elucidation were acquired at 15°C on a Varian Unity 600 MHz spectrometer using sequences from the ProteinPack package available online from the Varian user library. All NMR experiments were processed using nmrPipe [24] and visually analyzed and manipulated with the locally developed program Sparky 3 (Tom Goddard and Don Kneller, University of California, San Francisco, CA, USA).

2D-^{15}N-heteronuclear single quantum coherence spectra (HSQC), 3D-HNCACB, 3D-CBCA(CO)NH experiments were used to assign all amide ^1H, amide ^{15}N, $^{13}C\alpha$ and $^{13}C\beta$ resonances following standard techniques for backbone assignments [25,26]. 2D-^{13}C-HSQC with the carrier frequency centered in the ^{13}C aliphatic region, 3D-C(CO)NH, 3D-HC(CO)NH and 3D-HCCH-correlation spectroscopy spectra were then used to assign the remaining aliphatic side chain ^1H and ^{13}C resonances. Aromatic side chain resonances were also assigned by using a 2D-^{13}C-HSQC spectrum centered in the ^{13}C aromatic region and by inspecting cross-peak connectivities in 2D- and 3D-nuclear Overhauser enhancement spectroscopy (NOESY) experiments.

Restraints for structural calculation were extracted from three 3D-NOESY experiments: a NOESY-^{15}N-HSQC spectrum and two NOESY-^{13}C-HSQC spectra, one centered in the ^{13}C aliphatic region and the other in the ^{13}C aromatic region. All NOESY experiments were acquired using a 200 ms mixing time to allow NOE intensities to build up. The program Sparky was used to measure the volumes of NOE cross-peaks by integration. A total of 481, 880 and 128 NOE cross-

Table 1
Constraint and structural statistics

No. of NOE distance restraints	
Intraresidue ($i=0$)	120
Short-range ($i=1$)	346
Medium-range ($1<i<4$)	268
Long-range ($i>4$)	282
Total	1016
Pairwise rmsd for overlays (Å) (backbone, heavy)[a]	
6–47	0.25, 0.75
7–46	0.20, 0.73
7–25	0.23, 0.83
26–46	0.05, 0.59
Ramachandran plot region[b]	
In favored (%)	63.9
In additional allowed (%)	35.0
In generously allowed (%)	1.1
Restraint satisfaction	
rms violation (Å)	0.041 ± 0.0001
Maximum NOE violation	0.286
Average no. of NOE violations	23

[a]MOLMOL [40] was used to determine rmsd values for overlays.
[b]Procheck-NMR [41] was used to generate Ramachandran plots to assess the quality of the structures.

peak volumes were extracted from the NOESY-^{15}N-HSQC, NOESY-^{13}C-aliphatic-HSQC and NOESY-^{13}C-aromatic-HSQC spectra, respectively. The CALIBA macro of DYANA 1.5 [27] was then used to convert the integrated volumes to upper distance limits. Pseudo-atom corrections were introduced where stereospecific assignments were not available [28]. Lower bounds were also added to help define the structure and were conservatively set to 2.0 Å below the corresponding upper bounds. Furthermore, during the structural refinement process, negative restraints (lower bounds set to 4.0 Å for proton pairs that show no NOE cross-peaks in the spectra) were also introduced to eliminate unrealistic close contacts found in preliminary structures [29,30].

These upper and lower bounds were used in DYANA 1.5 [31] and AMBER-6 [32] to refine the structure of sTva47. One hundred structures were first calculated with DYANA using a simulated annealing cycle of 10 000 torsion angle dynamic steps to yield each structure. The 20 structures with the lowest target function were imported into AMBER and further refined by running several consecutive cycles of simulated annealing. The first six simulated annealing cycles were 60 ps long with 12 ps high temperature periods at 1000 K to help overcome local energy barriers. These were followed by nine consecutive 100 ps long annealing cycles with 20 ps spent at 1000 K, for a total of 15 annealing cycles and 1260 ps of AMBER molecular dynamic simulations. At the end of each cycle, the experimental distance restraints were analyzed against the calculated structures to identify and correct errors in assignments, integration and underestimated upper bounds due to spin diffusion. The last frame of the annealing cycle was then used to restart a new cycle using the newly refined set of distance bounds. Details of the final set of restraints are shown in Table 1 and Fig. 2D. The final structures were obtained by averaging the coordinates saved during the last 5 ps of equilibration at 300 K of the last annealing cycle and restrained energy minimized. The force constant used in AMBER for NOE distance restraints was 20 kcal/mol; this value was increased to 100 kcal/mol during high temperature dynamics at 1000 K. During AMBER calculations, a generalized Born implicit solvation model [33] was used to account for the effects of water solvation during molecular dynamic simulations, with the salt concentration set to the actual ion strength of our sample.

NOE cross-peak connectivities and preliminary structural calculations suggested a unique disulfide bonding pattern in agreement with the topology suggested by mutagenic studies [9] and comparison to other LDLR LBrs. Hence, the three disulfide bonds were defined for further structural calculations with DYANA and AMBER. On the contrary, calcium was not explicitly included as well as no dihedral angle restraints were used during our simulations. Moreover, the first five residues of sTva47 (I5–G9), that show only intraresidue and short-range NOE contacts, were poorly defined in early calculated structures and were not included in the calculations that yielded our final structures. The 20 lowest energy structures of the predominant conformer of sTva47 have been deposited in the Protein Data Bank (PDB), along with the NMR constraints and chemical shift assignments (PDB ID code 1K7B).

3. Results and discussion

3.1. sTva47 requires calcium for folding, structure and function

Purified sTva47 required oxidative folding to form the correct disulfide bonds. As was found for oxidation of LBr from the LDLR family of receptors [12,17,18,20], calcium was required to selectively form a single disulfide bonding pattern, which we assumed matched that of the native Tva and the LDLR LBr as previously suggested [9] (Wang et al. have reported similar findings [23]). After suitable conditions were defined, oxidation was carried out using purified MBP–sTva47 in order to use correctly oxidized sTva47 attached to MBP for surface plasmon resonance binding experiments (see below).

Inspection of ^{15}N-HSQC spectra revealed that the addition of excess (5 mM) calcium dramatically reduces the number (from >120 to 84) and increases the dispersion of cross-peaks in ^{15}N-edited HSQC spectra (data not shown). This indicates that, even when correctly oxidized, the Tva LBr requires bound calcium to stabilize its tertiary structure. Similar results were also found by Wang et al. for Tva [23] and for LBr of the LDLR family of receptors [12,17,18,20].

ALSV binds to its cellular receptor through the surface subunit (SU) of its envelope glycoprotein (Env). To quantitatively address the ability of sTva47 to bind ALSV-A Env, we performed surface plasmon resonance binding experiments using a previously characterized ALSV-A SU-immunoadhesin (SU(A)-rIgG) fusion [14]. In the absence of calcium (i.e. 2.5 mM EDTA) the binding constant was 5.5 nM. Notably, the presence of 5 mM calcium increased the affinity of this interaction 27.5-fold ($K_d = 0.2$ nM) (data not shown). This range of disassociation constants is similar to those previously reported, where the presence of calcium was not quantified [14,34]. These results demonstrate that calcium increases the affinity of sTva47 for the SU of ALSV-A, presumably by stabilizing its tertiary structure, as detailed below. This requirement for calcium for oxidative folding, structural stability, and receptor binding is consistent with the results of studies of LBr from the LDLR family of receptors [12,16–18,20–22].

3.2. Structural characterization of sTva47

Surprisingly, the ^{15}N-HSQC spectrum of properly folded sTva47 acquired in the presence of excess calcium shows a larger number of cross-peaks than expected (Fig. 2A), indicating the presence of multiple conformations which do not interconvert within the NMR time scale. Changes in the pH, protein concentration, salt concentration (including calcium concentration) and temperature (15–35°C range) of the sample did not seem to favor one set of cross-peaks over others.

Resonance assignments revealed three sets of cross-peaks for some residues indicating the presence of three different conformers (Fig. 2A). Plotting the chemical shift difference between the three conformers for each residue (Fig. 2B) showed that this conformational flexibility is localized to the loop region between C18 and C28 with the largest deviations found around two adjacent proline residues: P21 and P22. This observation suggested that a *cis–trans* isomerization

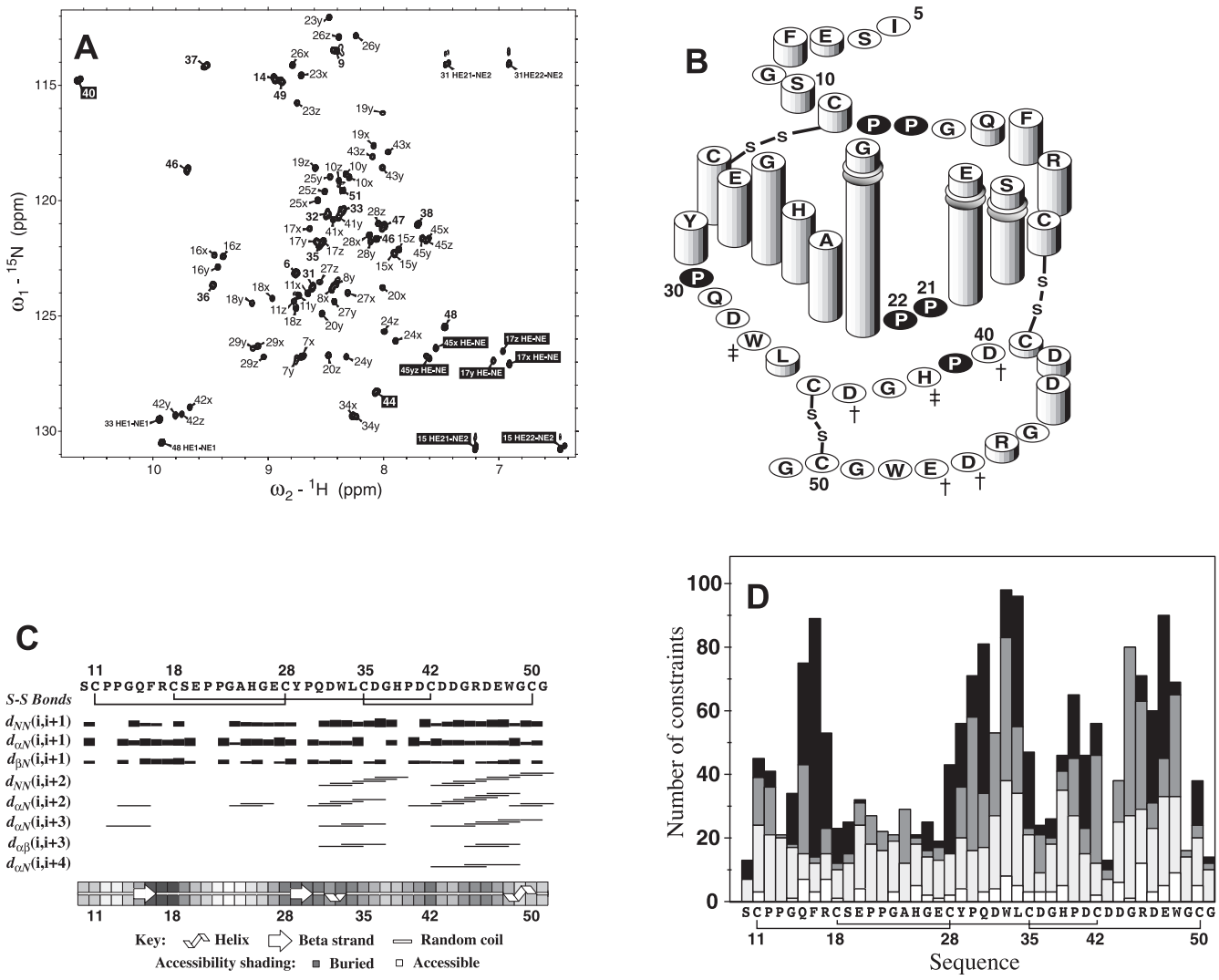

Fig. 2. A: ^{1}H–^{15}N HSQC spectrum of sTva47 with assignments. The three different conformers observed for some residues are labeled *x*, *y* and *z*, where *x* refers to the dominant *trans–trans* conformer whose structure was solved. Cross-peaks from side chain groups were also assigned and are explicitly labeled in the figure. Folded peaks are shown with black labels. B: Cartoon representation of sTva47 molecule with disulfide bonds and daggers to indicate residues that are involved in calcium coordination (‡, coordination by backbone carbonyl; †, coordination by side chain carboxyl). The height of the amino acid cylinders is proportional to the chemical shift difference between the three *x*, *y*, *z* conformers. C: Summary of local constraints used in deriving the structure of sTva47 including disulfide bonds and short- to medium-range NOE-derived backbone constraints. Secondary structure and average estimated accessibility are shown at the bottom as well. D: Plot of intra-residue, short-range ($i=1$), medium-range ($1<i<4$) and long-range ($i>4$) NOE distance restraints per residue.

equilibrium about the peptide bonds of P21 and P22 may be responsible for the multiple conformers. This hypothesis was demonstrated and the configuration of the two peptide bonds in the three conformers determined by analyzing Hα(*i*)–Hα(*i*+1) and Hα(*i*)–Hδ(*i*+1) NOE connectivities between residues E20–P21 and P21–P22. The conformers were found to have *trans–trans*, *trans–cis* and *cis–trans* configuration about the P21 and P22 peptide bonds, respectively, with the *trans–trans* conformer being the most abundant one, based on the relative intensities of ^{15}N-HSQC cross-peaks. In this manuscript we report the structure of the predominant *trans–trans* conformer. We note that this conformational flexibility seems to be restricted to the C18–C28 loop in the N-terminal half of Tva, far away from the putative binding site of the viral envelope glycoprotein. Moreover, the two proline residues undergoing *cis–trans* isomerization have been mutated without impairing the ability of Tva to function as a receptor for ALSV-A [35–37]. Thus, we conclude that while this prolyl isomerization process is a significant structural property of the quail Tva, it does not play an important role in viral receptor functionality.

In general, the root mean square deviation (rmsd) values, energies, geometry and Ramachandran statistics are good for all the calculated structures of sTva47 (Table 1). The structure appears to be formed from N- and C-terminal structural domains. The N-terminal domain is folded around the side chain of R17 (that has NOE contacts to 14 other residues) and is dominated by the C18–C28 loop with a short two strand parallel β-sheet at its bottom, also described in other LDLR LBr structures. This loop, which undergoes the isomerization process described above, is highly exposed to solvent and less well defined by NMR restraints. The C-terminal domain, on the other hand, appears to be better defined with a larger number of distance restraints, probably due to the stabilizing

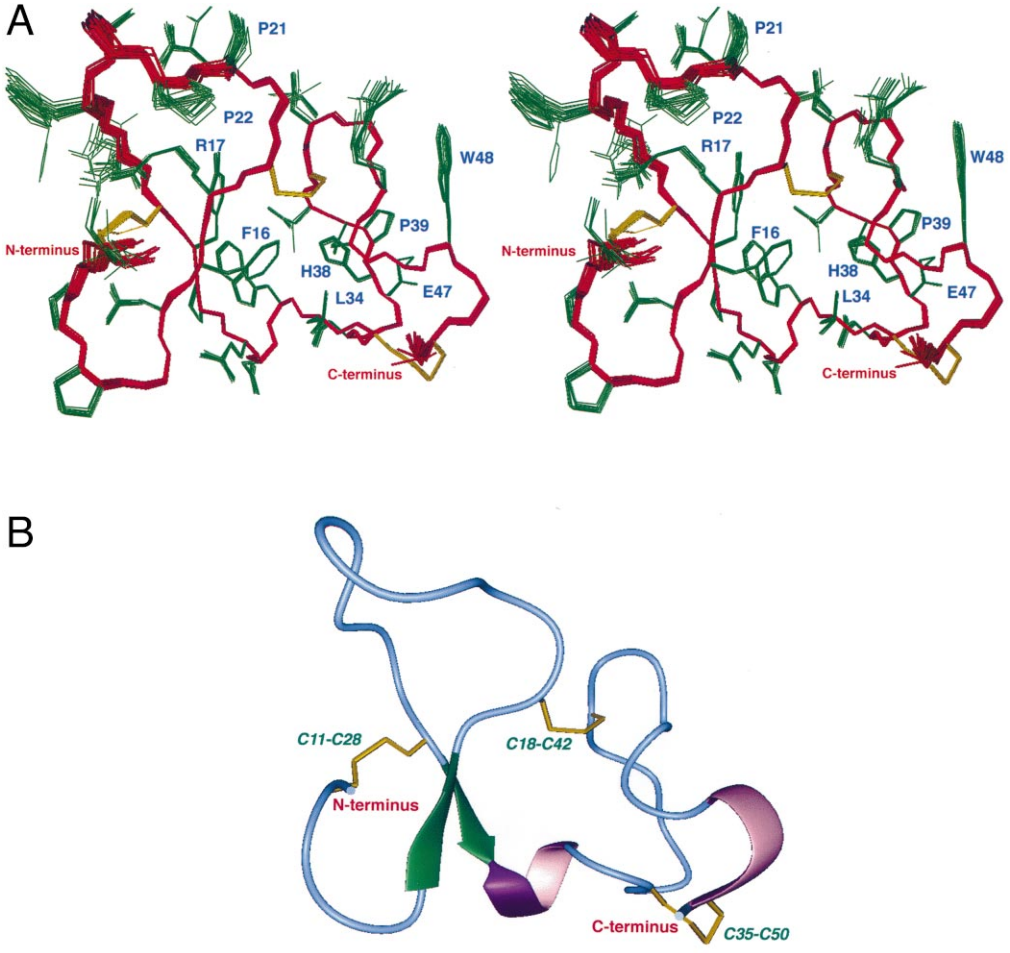

Fig. 3. A: Stereo view of the 20 lowest energy structures of sTva47 superimposed. Backbone atoms (red) are illustrated along with side chains (green). Disulfide bonds are shown in yellow. B: Lowest energy structure of sTva47 with secondary structural elements. This figure was prepared with the program MOLMOL [40].

effect of calcium coordination (Table 1 and Figs. 2 and 3). The two domains are linked together by the C18–C41 disulfide bond at one end and the backbone of residues Q31–L34, that form a short 3_{10}-helix (also found in other LDLR LBr), at the other end. In between these is the hydrophobic core of the protein comprised of the side chains of residues F16, Y29, P30 and W33. Another short 3_{10}-helix (residues W48–C50) is found at the C-terminus.

The structure of sTva47 was compared to LR5 [21], the fifth repeat of LDLR, chosen to represent the LBr fold. Not surprisingly, given the !!identical S–S topology and the putative calcium binding site, the structures are very similar with the backbone of the C-terminal and part of the N-terminal domains of sTva47 (residues C28–C50) overlapping to 1.0 Å of the corresponding LR5 residues (C17–C39) (Fig. 4A). Moreover, the rmsd value decreases to 0.6 Å if only the C-terminal domain is considered (L34–G49 of sTva47 overlapped to R23–N38 of LR5). The main differences between the structures are in the N-terminal domain, mainly because of the 5 aa longer C18–C28 loop found in sTva47 compared to LR5. This is also the region of Tva that undergoes prolyl isomerization.

The acidic side chains of D36, D40, D46 and E47, and the two backbone carbonyl oxygen atoms from residues L34 and H38, are correctly positioned by the NMR restraints to coordinate calcium. Together they form an octahedral cage, closely resembling the calcium binding site found in LR5 (Fig. 4B). The distances between opposing oxygen atoms are somewhat longer than expected, $\sim$7 Å compared to $\sim$5 Å, probably because of electrostatic repulsion between their negative charges in the absence of an explicit calcium atom during structural calculations. Given this finding and the important role that calcium plays in viral receptor function described earlier, we conclude that the calcium binding site found in LDLR LBr is conserved in Tva.

3.3. Implications for viral receptor function

Gain and loss of function studies have pointed to residues that are important or critical for Tva to act as an ALSV-A

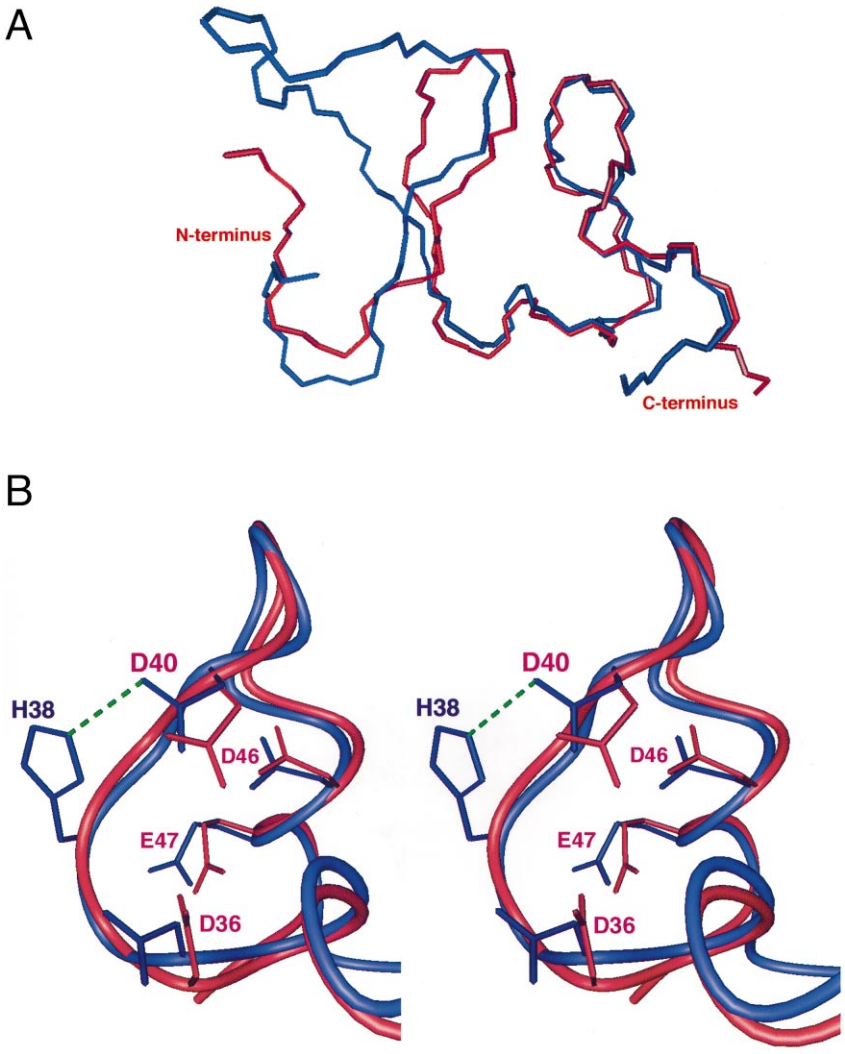

Fig. 4. A: Comparison of the backbone atom coordinates of sTva47 (light blue) and LR5 (red), the fifth repeat of LDLR that was chosen as representative of the LBr domain fold (residues 24–46 of sTva47 were superimposed to residues 17–39 of LR5). B: Comparison of the calcium binding sites of sTva47 and LR5. The H-bond formed between H38 and D40 of Tva is also shown in green. The coordinates of LR5 were obtained from the PDB (1ajj). Structural comparisons were performed using the program MOLMOL [40].

receptor. Most of these residues are located in the C-terminal portion of the protein suggesting that this is where the bulk of the viral binding site is located. Among them are highly conserved residues that are critical to ensure proper folding of the LBr module of Tva: D46 and E47, whose acidic side chains coordinate calcium [23,37], and C35 and C50, that form a disulfide bridge [9]. Mutations of these residues most likely exert their effect by disrupting the Tva structure at the viral binding site.

Other important amino acids (W48, G49, L34 and H38) are not conserved within the LBr family and may play a more direct role in viral receptor function. Perhaps one of the most interesting of these residues is W48 [13,14,35,37]. Our sTva47 structure shows the aromatic side chain of W48 at the surface of the protein, lying flat against the backbone and side chain of R45 (whose $^{1}H\alpha$ resonance is shifted upfield to 2.1 ppm due to its proximity to the aromatic ring) and to a lesser extent residues D43 and G44. Its position is well defined by NMR restraints. Given its exposed location, it is unlikely that W48 is critical for protein folding and, hence, its functional importance is most likely to derive from a direct interaction with the viral envelope glycoprotein. Furthermore, the presence of a glycine residue adjacent to W48 was also found to be important for function. While it was hypothesized that a bulkier side chain might interfere with the correct placement of the W48 aromatic side chain [36], our structure shows that position 49 could easily host a bulkier side chain without altering the conformation of W48. An alternative explanation is that G49 forms part of the binding surface and its mutation sterically interferes with Tva contacting the envelope glycoprotein. This is confirmed by the fact that the insertion of two amino acid residues after G49 (as found in LDLR LB1 and LB4) also disrupts viral receptor function [36], as if altering the binding surface.

L34, which some studies found to be critical for Tva receptor function [35,37], seems to play an important role for protein folding, since, as expected [23], it is mostly buried in the hydrophobic core of the protein. However, together with the highly conserved residue F16, L34 also forms a hydrophobic patch on the surface of Tva that is adjacent to W48 and may contact Env-A directly.

Finally, gain of function experiments using a bone fide

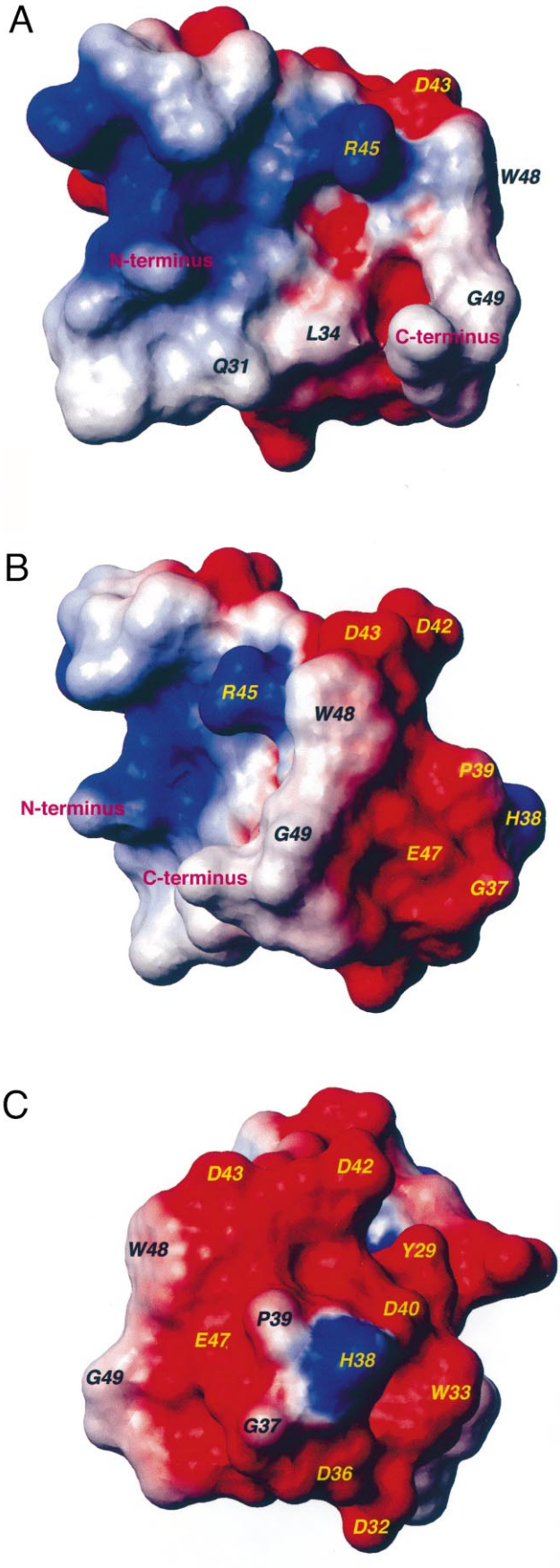

Fig. 5. A–C: Molecular surface of the sTva47 structure colored by electrostatic potential. In B and C, the modules are rotated ~90° around the vertical axis. This figure was prepared with the program MOLMOL [40].
←

LDLR repeat also pointed to H38 playing a role in viral receptor function [36]. This residue is not conserved among LBrs and in our structure is at the surface of Tva suggesting that it interacts directly with the envelope glycoprotein. H38, however, also seems to be important for calcium coordination, as it provides one of the two backbone carbonyl oxygen atoms that bind calcium and its aromatic side chain forms a H-bond to the acidic side chain of D40, which also coordinates the calcium ion (Fig. 4B).

Although most of the work done so far points to the viral binding site being near the C-terminus of the Tva LBr domain, there have been indications that residues from the N-terminal domain of the molecule may also play a minor role in viral receptor function [37]. In a recent report, three mutations in the hr1 region of the SU subunit of Env-A, E149K, Y142N and Y142N/E149K, were found to reduce the binding affinity for quail but not chicken sTva [38]. Since the C-terminal halves of chicken and quail Tva are identical, these results point to a positively charged residue present in the quail but not chicken N-terminal domain of Tva that contacts the hr1 region of Env-A (Fig. 1). A possible candidate is H25, which is Gln in the chicken sequence. Our structure, however, shows that the H25 side chain is located on the opposite side of the molecule far away from the putative SU binding surface. The only other positively charged residue found in the quail but not chicken sequence is R10, surprisingly just outside the LBr domain (Gln in the chicken sequence). Unfortunately our sequence differs from both quail and chicken in that it has a Ser at this position. Furthermore, in our structure this Ser is poorly defined both because its exposure at the surface and its proximity to the disordered N-terminus. However, it is quite plausible that an Arg residue at this position could contact Env-A directly. While this interaction may not contribute significantly to Tva-SU binding affinity, Env mutations like the ones described above could readily introduce steric or electrostatic clashes capable of disrupting binding of quail Tva to Env-A.

3.4. Analysis of Tva surface

Inspection of the molecular surface of Tva reveals a hydrophobic patch at the C-terminus, composed of residues W48 and G49, that extends towards the N-terminal domain with L34, Q31 and F16 (Fig. 5A). The other side of the C-terminal domain is highly polar (Fig. 5B,C) with the positively charged H38 residue surrounded by negatively charged acidic side chains. The viral binding site is most likely centered around residues W48–G49, extending on one side towards H38 and on the other towards the hydrophobic patch formed by L34 and F16. In between W48, G49 and H38 we find the acidic side chain of E47 which also coordinates calcium. Being located in such a hot spot at the Tva surface suggests that E47 may also play a more direct role in viral receptor function, perhaps by interacting with those basic residues on the hr2 region of Env-A that mutagenic studies found to be important for Tva binding [39].

4. Conclusions

We have functionally and structurally characterized sTva47, a 47 aa peptide that contains the LBr domain of Tva that is sufficient and necessary to interact with ALSV-A and trigger a change in conformation of Env. The 3D structure of sTva47 is remarkably similar to that of other LBr domains, with identical S–S topology and a conserved calcium binding site near the C-terminus. Furthermore, all the residues that are known to be important for viral receptor function are clustered in the C-terminal half of the molecule. These findings explain our observations that calcium is required for oxidative folding, structural stability and also its ability to increase the affinity of Tva for Env-A. Finally, surface analysis points to a putative binding site in the C-terminal domain of Tva where important and critical residues (W48, G49, H38, L34 and E47) are exposed at the surface and likely to interact directly with the viral envelope glycoprotein.

Acknowledgements: We thank Dr. A. Weiss (UCSF/HHMI) for use of a BIAcore, Dr. C. Turck (UCSF/HHMI) for use of a LCQ (Finnigan) mass spectrometer, Dr. J.A.T. Young (Harvard Med) for providing SU(A)-rIgG, Dr. T.M. Handel for use of a Bruker DMX 600 MHz spectrometer for preliminary NMR analysis, Dr. V. Basus for help acquiring NMR experiments on a Varian Unity 600 MHz spectrometer and Dr. C. Kojima for helpful discussions. This work was supported by the Howard Hughes Medical Institute and NIH Grant GM39247 (T.L.J.).

References

[1] White, J.M. (1992) Science 258, 917–924.
[2] Carr, C.M., Chaudhry, C. and Kim, P.S. (1997) Proc. Natl. Acad. Sci. USA 94, 14306–14313.
[3] Bullough, P.A., Hughson, F.M., Skehel, J.J. and Wiley, D.C. (1994) Nature 371, 37–43.
[4] Mothes, W., Boerger, A.L., Narayan, S., Cunningham, J.M. and Young, J.A.T. (2000) Cell 103, 679–689.
[5] Vogt, P.K. (1977) in: Comprehensive Virology (Fraenkel-Conrat, H. and Wagner, R., Eds.), Vol. 9, pp. 341–455, Plenum, New York.
[6] Bates, P., Young, J.A.T. and Varmus, H.E. (1993) Cell 74, 1043–1051.
[7] Young, J.A.T., Bates, P. and Varmus, H.E. (1993) J. Virol. 67, 1811–1816.
[8] Rong, L. and Bates, P. (1995) J. Virol. 69, 4847–4853.
[9] Belanger, C., Zingler, K. and Young, J.A.T. (1995) J. Virol. 69, 1019–1024.
[10] Bieri, S., Djordjevic, J.T., Daly, N.L., Smith, R. and Kroon, P.A. (1995) Biochemistry 34, 13059–13065.
[11] Bieri, S., Djordjevic, J.T., Jamshidi, N., Smith, R. and Kroon, P.A. (1995) FEBS Lett. 371, 341–344.
[12] Blacklow, S.C. and Kim, P.S. (1996) Nat. Struct. Biol. 3, 758–761.
[13] Hernandez, L.D., Peters, R.J., Delos, S.E., Young, J.A.T., Agard, D.A. and White, J.M. (1997) J. Cell Biol. 139, 1455–1464.
[14] Zingler, K. and Young, J.A.T. (1996) J. Virol. 70, 7510–7516.
[15] Goldstein, J.L. and Brown, M.S. (1974) J. Biol. Chem. 249, 5153–5162.
[16] Atkins, A.R., Brereton, I.M., Kroon, P.A., Lee, H.T. and Smith, R. (1998) Biochemistry 37, 1662–1670.
[17] North, C.L. and Blacklow, S.C. (1999) Biochemistry 38, 3926–3935.
[18] Dolmer, K., Huang, W. and Gettins, P.G.W. (1998) Biochemistry 37, 17016–17023.
[19] North, C.L. and Blacklow, S.C. (2000) Biochemistry 39, 2564–2571.
[20] Bieri, S., Atkins, A.R., Lee, H.T., Winzor, D.J., Smith, R. and Kroon, P.A. (1998) Biochemistry 37, 10994–11002.
[21] Fass, D., Blacklow, S., Kim, P.S. and Berger, J.M. (1997) Nature 388, 691–693.
[22] Huang, W., Dolmer, K. and Gettins, P.G.W. (1999) J. Biol. Chem. 274, 14130–14136.
[23] Wang, Q.-Y., Dolmer, K., Huang, W., Gettins, P.G.W. and Rong, L. (2001) J. Virol. 75, 2051–2058.
[24] Delaglio, F., Grzesiek, S., Buister, G.W., Zhu, G., Pfeifer, J. and Bax, A. (1995) J. Biomol. NMR 6, 277–293.
[25] Clore, G.M. and Gronenborn, A.M. (1991) Science 252, 1390–1399.
[26] Clore, G.M. and Gronenborn, A.M. (1998) Curr. Opin. Chem. Biol. 2, 564–570.
[27] Guntert, P., Braun, W. and Wuthrich, K. (1991) J. Mol. Biol. 217, 517–530.
[28] Wüthrich, K., Billeter, M. and Braun, W. (1983) J. Mol. Biol. 169, 949–961.
[29] Yao, L.J., James, T.L., Kealey, J.T., Santi, D.V. and Schmitz, U. (1997) J. Biomol. NMR 9, 229–244.
[30] Schmitz, U., Donati, A., James, T.L., Ulyanov, N.B. and Yao, L. (1998) Biopolymers 46, 329–342.
[31] Guntert, P., Mumenthaler, C. and Wuthrich, K. (1997) J. Mol. Biol. 273, 283–298.
[32] Cornell, W.D. et al. (1995) J. Am. Chem. Soc. 117, 5179–5197.
[33] Tsui, V. and Case, D.A. (2000) J. Am. Chem. Soc. 122, 2489–2498.
[34] Balliet, J.W., Berson, J., D'Cruz, C.M., Huang, J., Crane, J., Gilbert, J.M. and Bates, P. (1999) J. Virol. 73, 3054–3061.
[35] Zingler, K., Belanger, C., Peters, R.J., Agard, D.A. and Young, J.A.T. (1995) J. Virol. 69, 4261–4266.
[36] Rong, L., Gendron, K. and Bates, P. (1998) Proc. Natl. Acad. Sci. USA 95, 8467–8472.
[37] Rong, L., Gendron, K., Strohl, B., Shenoy, R., Wool-Lewis, R.J. and Bates, P. (1998) J. Virol. 72, 4552–4559.
[38] Holmen, S.L., Melder, D.C. and Federspiel, M.J. (2001) J. Virol. 75, 726–737.
[39] Rong, L., Edinger, A. and Bates, P. (1997) J. Virol. 71, 3458–3465.
[40] Koradi, R., Billeter, M. and Wuthrich, K. (1996) J. Mol. Graph. 14, 51–55.
[41] Laskowski, R.A., Rullmannn, J.A., MacArthur, M.W., Kaptein, R. and Thornton, J.M. (1996) J. Biomol. NMR 8, 477–486.